

## Article

# A Methodology to Estimate Single-Event Effects Induced by Low-Energy Protons

Cleiton Marques <sup>1,\*</sup>, Frédéric Wrobel <sup>1</sup>, Ygor Aguiar <sup>2</sup>, Alain Michez <sup>1</sup>, Jérôme Boch <sup>1</sup>, Frédéric Saigné <sup>1</sup> and Rubén García Alía <sup>2</sup>

<sup>1</sup> Institut d'Electronique et des Systèmes (IES), UMR-CNRS 5214, University of Montpellier, 34095 Montpellier, France; frederic.wrobel@umontpellier.fr (F.W.); alain.michez@umontpellier.fr (A.M.); jerome.boch@umontpellier.fr (J.B.); frederic.saigne@umontpellier.fr (F.S.)

<sup>2</sup> European Organization for Nuclear Research (CERN), CH-1211 Geneva, Switzerland; ygor.aguiar@cern.ch (Y.A.); ruben.garcia.alia@cern.ch (R.G.A.)

\* Correspondence: cleiton-magano.marques@umontpellier.fr

**Abstract:** This work explains that the Coulomb elastic process on the nucleus is a major source of single-event effects (SEE) for protons within the energy range of 1–10 MeV. The infinite range of Coulomb interactions implies an exceptionally high recoil probability. This research seeks to extend the investigations under which the elastic process becomes significant in the energy deposition process by providing a simplified methodology to evaluate the elastic contribution impact on the reliability of electronics. The goal is to derive a method to provide a simple way to calculate and predict the SEE cross-section. At very low energy, we observe a significant increase in the proton differential cross-section. The use of a direct Monte Carlo approach would mainly trigger low energy recoiling ions, and a very long calculation time would be necessary to observe the tail of the spectrum. In this sense, this work provides a simple methodology to calculate the SEE cross-section. The single-event upset (SEU) cross-section results demonstrate a good agreement with the experimental data in terms of shape and order of magnitude for different technological nodes.

**Keywords:** single-event effects; SEU; proton; cross-section; elastic process; Coulomb interaction



**Citation:** Marques, C.; Wrobel, F.; Aguiar, Y.; Michez, A.; Boch, J.; Saigné, F.; García Alía, R. A Methodology to Estimate Single-Event Effects Induced by Low-Energy Protons. *Eng* **2024**, *5*, 319–332. <https://doi.org/10.3390/eng5010017>

Academic Editor: Antonio Gil Bravo

Received: 15 December 2023

Revised: 16 February 2024

Accepted: 17 February 2024

Published: 19 February 2024



**Copyright:** © 2024 by the authors. Licensee MDPI, Basel, Switzerland. This article is an open access article distributed under the terms and conditions of the Creative Commons Attribution (CC BY) license (<https://creativecommons.org/licenses/by/4.0/>).

## 1. Introduction

The downscaling of electronic devices has significantly increased the sensitivity to low-energy particles such as neutrons and protons [1–5]. These particles belong to the family of hadrons and can provoke single event effects (SEE) by generating secondary ions that ionize the silicon in the device. These secondary ions arise from nuclear reactions initiated by the strong force interactions (hadronic process) [6]. There are similarities between neutrons and protons, which generally lead us to consider that electronic devices have the same sensitivity to both types of particles, at least above a few tens of MeV [7]. However, protons can also generate recoil ions through Coulomb interactions [8,9].

Considering SEE, memory devices are one of the most sensitive components, being prone to single-event upsets (SEU). In this sense, the sensitivity of memory devices to radiation effects, particularly regarding proton irradiation, has been extensively studied over the years [10–13]. This analysis reveals two main mechanisms driving single-event upset (SEU) sensitivity: direct ionization for low-energy protons (1 MeV) [12,13] and nonelastic nuclear reactions for high-energy protons (>10 MeV) [14,15]. Recent research has highlighted the significant contribution of the Coulomb elastic process between the 1 and 10 MeV energy range [8,11]. The probability of elastic recoil occurring is exceptionally high due to the infinite range of the Coulomb interactions.

In [8], a detailed analysis was performed, providing equations to calculate the SEE cross-section related to the silicon recoils through elastic scattering. However, this approach becomes complex if the user does not have in-depth knowledge of physics, electronics,

and particle-matter interaction. In [11], more integrated devices and configurations were evaluated to investigate the mechanisms induced by proton irradiation. However, this work used Monte Carlo simulations to model the proton interaction, which is not the ideal approach. Due to the divergence at low recoil energy (as will be discussed in the Section 3), a direct MC approach would trigger mainly low-energy recoil ions, and a very long calculation time would be required to observe the tail of the spectrum.

This work, carried out in the framework of the RADNEXT project [16], details the mechanisms of the elastic process and extends the analysis by providing an engineering tool to evaluate the electronics sensitivity to protons at low energy. The goal is to derive a method to provide a simple way to calculate and predict the SEE cross-section.

The paper is structured as follows: In Section 2, we present the background related to the nucleon interaction process and the main interaction processes below 10 MeV. In Section 3, we explain the methodology, modeling, and simulation of the proton cross-section, establishing the linear energy transfer (LET) distribution of ions reaching the sensitive region. In Section 4, SEU cross-section results are presented and compared with experimental data. Finally, in Section 5, we present the conclusions of the work.

## 2. Particle-Matter Interaction Background

To propose a method that calculates the SEE cross-section, we first need to better understand the processes that occur during the particle-matter interaction. When a proton or neutron interacts with a nucleus of an atom, three different processes can occur:

- Capture process—the incident proton or neutron is captured by the target nucleus, leading to the subsequent emission of gamma radiation to de-excite the resulting nucleus. Both particles require sufficient energy to initiate capture, and quantum mechanical effects further influence the probability, often resulting in relatively low capture probabilities. Additionally, the nuclear shell structure, which dictates the availability of energy states within the nucleus, can impact the probability of capture. Competing interactions, resonance effects, and isotope-specific properties contribute to this phenomenon. The low cross-section for neutron and proton capture results from intricate interplays between charge considerations, energy thresholds, quantum mechanics, nuclear structure, and isotope-specific behavior, demanding specific conditions and energies for these capture events to occur [17]. In this sense, we will not discuss this process in this work.
- Elastic process—the incident proton or neutron undergoes scattering by the target nucleus, resulting in the recoil of the target nucleus due to energy and momentum transfer. Figure 1 illustrates the elastic mechanism. The elastic scattering process involves the interaction of a nucleon with a target nucleus without any change in the system's internal energy, i.e., the conservation of total kinetic energy [18]. When a nucleon approaches a nucleus, it experiences a potential energy field due to the positive charge of the nucleus. If the nucleon has sufficient energy to overcome this potential barrier, it gets closer to the nucleus. During this interaction, the nucleon also exchanges energy and momentum with the nucleus, resulting in a change in direction for both particles. During this recoil, the ion generated can potentially trigger SEE [19,20].
- Nonelastic process—the incident proton or neutron can excite or fragment the target nucleus. Unlike the elastic process, there is no conservation of kinetic energy. This process often leads to the generation of secondary particles, including ions that can trigger failures in electronic devices [18]. Figure 2 illustrates the nonelastic mechanism. In this process, the target nucleus may absorb the nucleon, forming a new compound nucleus or initiating nuclear reactions. Alternatively, the nucleon may induce inelastic scattering, exciting the nucleus to a higher energy state before being emitted [18,20].

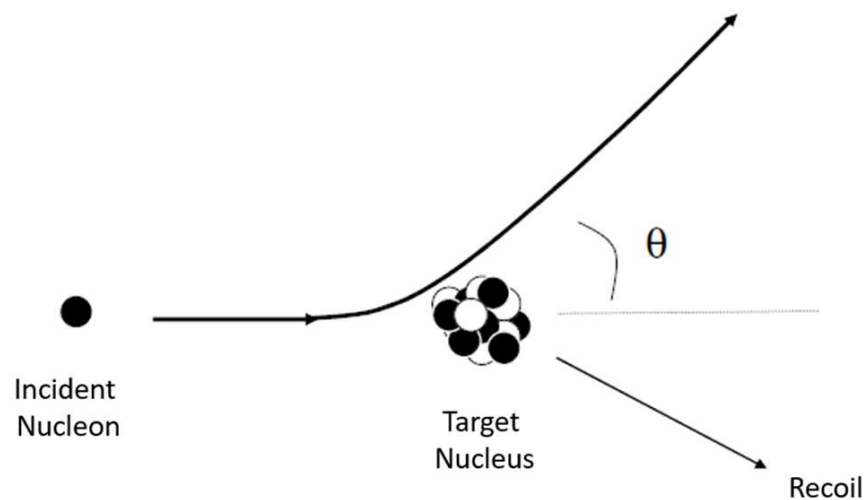


**Figure 1.** Elastic reaction leading to the deflection of the incident nucleon and the recoil of the target nucleus [18]. The recoil ion may be responsible for an SEE.

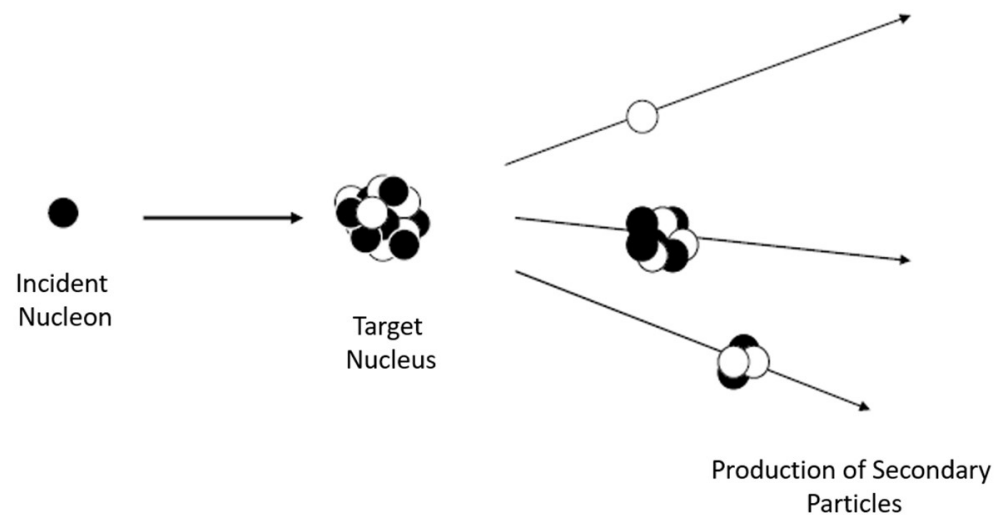


**Figure 2.** Nonelastic reaction leading to the production of secondary particles [18]. The secondaries may ionize the matter and trigger SEE.

However, unlike neutrons, protons are charged particles and can also interact directly with matter by the Coulomb force [8,11,18]. In this sense, there are two kinds of Coulomb interactions to consider:

- Coulomb interaction with the electrons—This interaction corresponds to the direct ionization of the primary proton when it interacts with the electrons of the medium. The process involves the transfer of energy from the proton to the electrons, leading to the ionization of the medium and potentially causing SEE in electronic devices [20,21].
- Coulomb interaction with the nuclei—In this elastic process, protons interact with the nuclei of the medium through the Coulomb force, resulting in the recoil of the impinging nucleus. This recoil can induce secondary ionization and contribute to the overall SEE rate in electronic devices. The total elastic process during proton–nucleus interaction is therefore attributed to the sum of two different processes: the strong force interaction and the Coulomb interaction [22].

#### *Main Process below 10 MeV*

Proton interaction processes are very similar to neutron ones. To understand the differences between neutrons and protons, identifying the contribution of each process, we

need to investigate the products of the reactions generated during the interaction of both particles with matter. For each kind of reaction that can occur, there is a different threshold energy that corresponds to the minimum energy required to generate the secondary products. Table 1 illustrates the possible reactions for neutrons and protons below 10 MeV.

**Table 1.** Reaction products as a function of incident energy for neutrons and protons in  $^{28}\text{Si}$  below 10 MeV.

Incident Particle	Reaction Products	Reaction Kind	Reaction Threshold (MeV)
Neutrons	$^{29}\text{Si} + \gamma$	capture	0
	$^{28}\text{Si} + n$	elastic	0
	$^{28}\text{Si} + n$		1.78
	$^{25}\text{Mg} + \alpha$	nonelastic	2.75
	$^{28}\text{Al} + p$		4.00
	$^{27}\text{Al} + d$		9.70
Protons	$^{29}\text{Si} + \gamma$	capture	0
	$^{28}\text{Si} + p$	elastic	0
	$^{25}\text{Al} + \alpha$	nonelastic	7.99

Based on Table 1, below 10 MeV, neutrons have four possible nonelastic reactions, while protons only have one. This is due to the charge of protons, which makes it more challenging to enter the nucleus and generate secondary ions. Looking at the only product generated by the proton, the aluminum production, it is insignificant for SEE contribution. This is shown in Figure 3, in which we plotted the reaction cross-section from the International Atomic Energy Agency (IAEA) database [23].

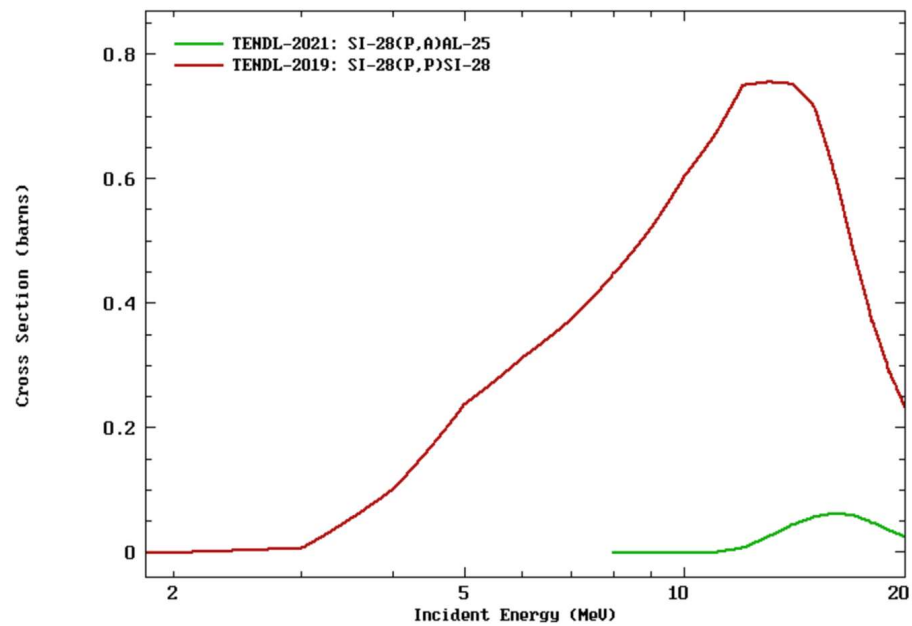


**Figure 3.** Nuclear cross-sections for  $p + ^{28}\text{Si}$  interaction. Data from IAEA database [23].

Finally, for protons below 10 MeV, the main process at play is the elastic reaction [8], which can be due to the strong force (hadronic process) and, at the same time, to the Coulomb force.

### 3. SEE Cross-Section Calculation Method

As discussed in the previous section, we know that the elastic reaction is essential for evaluating low-energy proton interactions. The next step is to develop a methodology to

calculate the proton SEE cross-section  $\sigma_p(E_p)$ . One way to evaluate it is using the heavy-ions cross-section experimental results  $\sigma_{HI}(LET)$  as a basis [24]. To determine  $\sigma_p(E_p)$ , we can write:

$$\sigma_p(E_p) = \int_0^{LET_{max}} \frac{dP(E_{th})}{dLET} \sigma_{HI}(LET) dLET \tag{1}$$

In Equation (1), the  $\frac{dP}{dLET}$  is the LET distribution of the recoiling ions and secondary products that are produced during nucleon transport in matter. The quantity  $LET_{max}$  is the maximum ion LET generated by the proton interaction with a given energy ( $E_p$ ). To calculate the LET distribution, we first need to obtain the cumulative probability  $P(E_{th})$  of a proton crossing a target material with a thickness ( $\Delta x$ ), the number of atoms per unit volume ( $N$ ), and the nuclear cross-section ( $\sigma_{prod}$ ). This probability is given by Equation (2) [18]:

$$P = 1 - e^{-N\sigma_{prod}\Delta x} \tag{2}$$

where  $N$  for silicon is  $5 \times 10^{22}$  atoms/cm<sup>3</sup>.

To continue with the development of the method, we must further investigate the nuclear elastic cross-section. At this point, it is important to highlight the difference between the SEE cross-section, which measures the device’s sensitive area, and the nuclear cross-section, which expresses the probability of a particle to produce a nuclear reaction.

### 3.1. Nuclear Elastic Cross-Section Analysis

To investigate the nuclear elastic cross-section  $\sigma_{prod}$  below 10 MeV, we simulated the interaction of neutrons and protons with a silicon nucleus using the DHORIN code [25]. DHORIN uses a spherical optical model and computes angular differential cross-section by using the ECIS code [26]. Then, by using basic equations of relativistic kinematics, DHORIN calculates the differential cross-section as a function of kinetic energy of the silicon recoil. Figures 4 and 5 present the resulting calculations for protons at 5 MeV and 10 MeV, respectively. For comparison, we represented the results together for neutrons in the same energy.

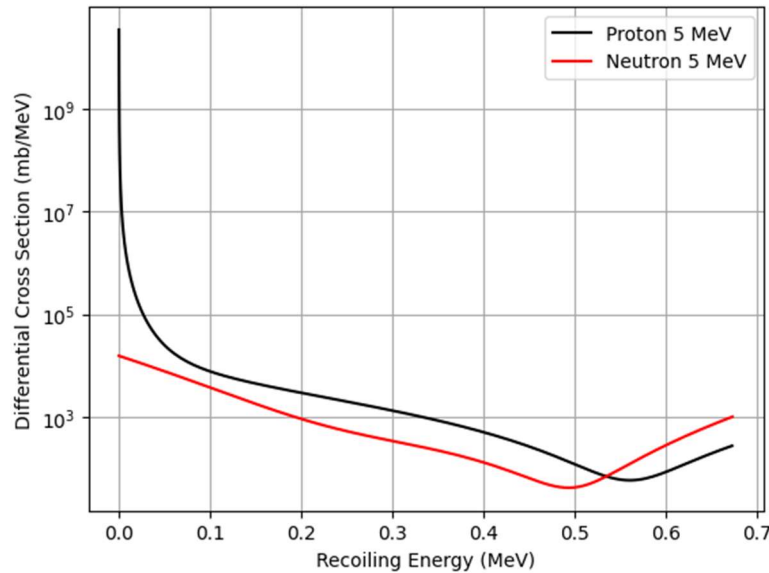


**Figure 4.** Differential cross-section for incident neutrons and protons at 5 MeV and as a function of recoiling energy.

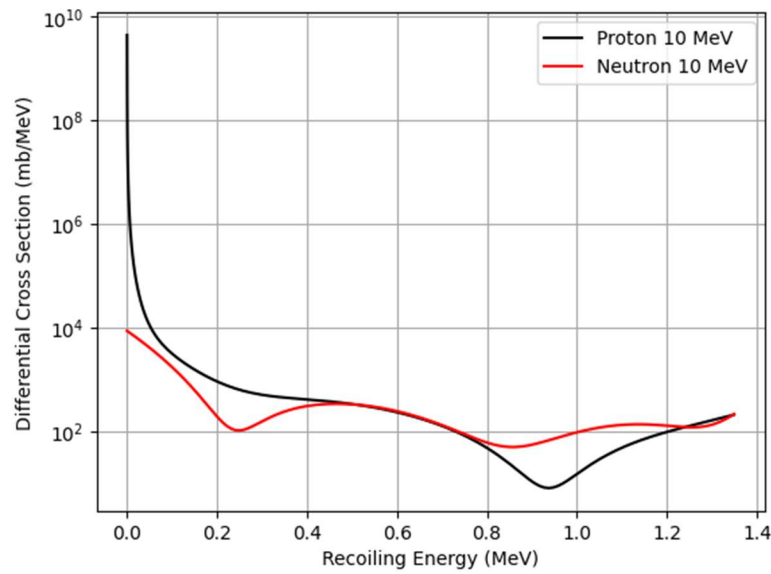


**Figure 5.** Differential cross-section for incident neutrons and protons at 10 MeV and as a function of recoiling energy.

Above 100 keV, neutrons and protons give two shapes that are very close as well as the order of magnitude of the differential cross-section. However, below 100 keV, we observe a very significant increase in the proton cross-section. This important difference is due to the Coulomb collision, which only exists for protons. At very low energies, the differential cross-section for protons is a million times greater than that of neutrons.

As the objective of this work is to estimate the proton SEE cross-section, it is crucial to determine a threshold energy ( $E_{th}$ ) beyond which the recoil ion can trigger a fault in the device. If we compare proton and silicon ions, the threshold energy is expected to be similar for both. For technologies that are sensitive to the direct ionization of protons, we can consider, in a first approximation, that the  $E_{th}$  is around the proton energy near the Bragg peak ( $E_{th} = 50$  keV), which corresponds to the maximum of the linear energy transfer (LET). In this sense, the recoil ion can trigger a fault if the energy is higher than the  $E_{th}$ . Figure 6 plots the elastic cross-section results for different values of threshold energy and as a function of the incident proton energy. Table 2 presents typical values of  $E_{th}$  for different technologies.

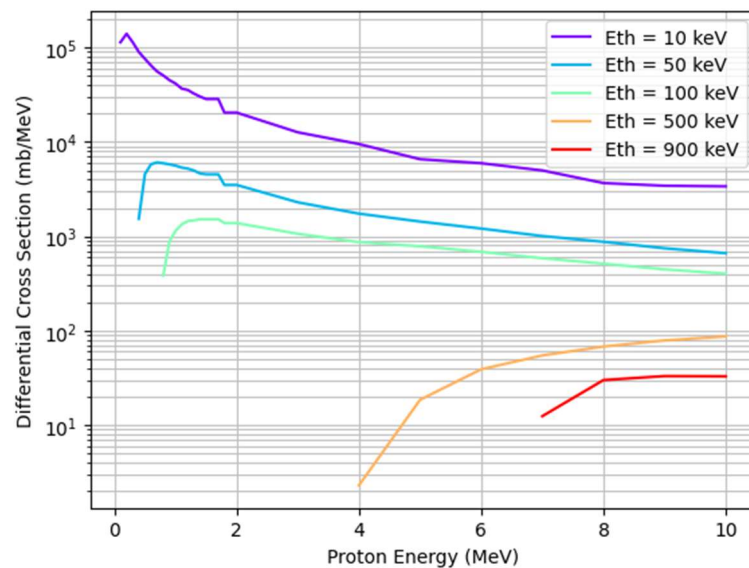


**Figure 6.** Elastic cross-section as a function of proton energy for different threshold recoil energies.

**Table 2.** Typical critical charge ( $Q_c$ ),  $LET_{th}$ , and  $E_{th}$  for different technologies [4].

Gate Length (nm)	$Q_c$ (fC)	$LET_{th}$ (MeV·cm <sup>2</sup> /mg)	$E_{th}$ (keV)
250	8	1.99	180
130	2.5	1.34	56
90	1.2	0.87	27
65	0.8	0.82	18

This analysis shows that low-energy proton interactions play a crucial role in the energy deposition in silicon, not just through direct ionization but also because of elastic reactions. However, this first approach does not account for the fact that recoils are not always produced in the sensitive volume (the *Si* substrate layer of the device) and can release some energy before reaching it, e.g., in the back-end of line (BEOL). As a result, we must consider that the differential cross-section is not the same at any point of the track.

### 3.2. Typical Ion Recoiling Ranges

To better understand the impact of the track, Table 3 summarizes the typical ranges of proton and silicon ions in silicon. The first line gives the values of the incident proton energy that we have considered. The second line gives the ranges of protons in silicon using the SRIM code [27]. The third line gives the maximum kinetic energy that a silicon recoil can have, which is calculated based on the differential cross-section results obtained with DHORIN. The last two lines were obtained using SRIM. Our methodology calculates the differential cross-section, which allows us to establish the relationship between the energy and nucleon diffusion angle. Since 180° is the highest angle that can be achieved, we can determine the maximum energy and calculate the maximum LET and range associated with this recoil.

**Table 3.** Typical recoiling ranges of ions in silicon.

Proton energy (MeV)	1	5	10
Proton range in <i>Si</i> (μm)	16	200	700
Maximum recoiling energy of <i>Si</i> (MeV)	0.13	0.68	1.30
Maximum LET of the recoil in <i>Si</i> (MeV·cm <sup>2</sup> /mg)	2.8	4.1	6.2
Maximum range of recoiling <i>Si</i> in <i>Si</i> (μm)	0.18	2.70	3.50

The main conclusion is that the recoiling ions must be generated in a small layer of BEOL before reaching the sensitive region. As an example, at 10 MeV, the recoiling silicon may have an energy up to 1.3 MeV and thus must be generated no further than 3.5 μm from the sensitive region to be able to reach the sensitive area. As the range of a proton is comparable to the BEOL thickness at low energy (a few MeV), it means that it is necessary to consider the energy loss of the primary proton before the elastic collision responsible for a recoiling *Si* that will provoke an SEE.

### 3.3. Energy Loss Modeling

To model the loss of energy, we simulate a structure composed of two layers of silicon. The first one represents the BEOL, and the second one represents the sensitive region located in the bulk. This is a first approximation, as the real BEOL is composed not only of silicon but of several different materials. However, the real composition of the BEOL is generally confidential, and here, we use a simplified structure. The thickness of the sensitive region is generally assumed to be of the order of magnitude of 1–2 μm, consistent with the diffusion process of the charges during the ionization. If a silicon ion recoils inside the sensitive region, we can estimate its initial LET by calculating the recoiling energy of the reaction. However, if the recoil is generated outside the sensitive region, we need to

take into account that the recoiling ion will lose energy before it reaches the sensitive region. This means that the effective LET value will be different from the initial one. Figure 7 illustrates the way a recoiling silicon can be generated at a distance  $x$  of the sensitive region.

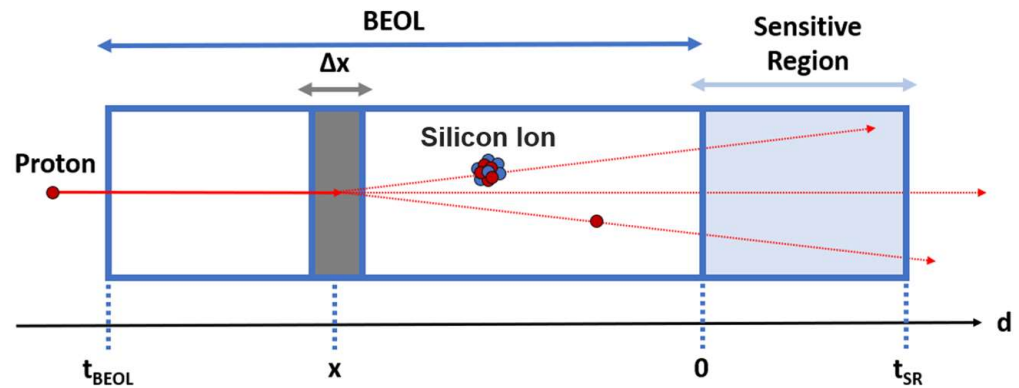


**Figure 7.** Illustration of an elastic collision in the BEOL. The recoiling silicon loses energy along its track and can reach the sensitive region with different LET.

The aim of our modeling is to determine the LET distribution of secondary ions that reach the sensitive region. Even if a Monte Carlo approach seems to be appropriate for this kind of calculation, it is not the optimal approach. Indeed, because of the divergence at low recoil energy (shown in Figures 4 and 5), a direct Monte Carlo approach would mainly trigger low-energy recoiling ions, and a very long calculation time would be necessary to observe the tail of the spectrum. To prevent this, we adopt an analytical approach in which we consider that, to reach the sensitive region with a LET greater than a given value, it can be produced in many positions in the structure. By using the SRIM code, it is then possible to calculate the nuclear cross-section for producing this kind of ion at any position and, thus, the probability to create it in a small layer. To run this analysis, we need to define the three input parameters, which are the incident proton energy ( $E_p$ ), the BEOL layer thickness ( $t_{BEOL}$ ), and the sensitive region thickness ( $t_{SR}$ ).

Based on this methodology, we extract the range functions of protons in silicon and silicon in silicon. Let  $R_p(E_p)$  be the range function of the proton and  $R_{Si}(E_{Si})$  the range function of the  $Si$  ion. These functions depend on the particle energy and can be easily determined with the SRIM code [28]. We also need the reciprocal functions  $R_p^{-1}$  and  $R_{Si}^{-1}$  that give the energy of a particle, knowing its range. The proton energy can thus be determined anywhere along the  $d$ -axis:

$$E_p(x) = R_p^{-1}(R_p(E_p(t_{BEOL})) - (t_{BEOL} - x)) \tag{3}$$

Now, for an ion produced at the position ( $x$ ) with an energy  $E_{Si}(x)$  to reach the sensitive region with an energy greater than the energy threshold ( $E_{th}$ ), we need to have:

$$E_{Si}(x; LET_{th}) = R_{Si}^{-1}(R_{Si}(E_{th}(LET_{th})) + x) \tag{4}$$

The  $E_{th}$  is calculated for different  $LET_{th}$  values based on the maximum LET of the recoil in  $Si$ . The next step is to calculate the cross-section ( $\sigma_{prod}$ ) to produce an ion at the position  $x$  with high enough energy to reach the sensitive region. We obtained it by integrating the recoiling distribution at  $E_p(x)$  between  $E_{Si}(x; LET_{th1})$  and  $E_{Si}(x; LET_{th2})$ . The probability that such an ion is created in the  $\Delta x$  layer is given by the Equation (2), as was presented at the beginning of this section.

By integrating over all the values of  $x$ , we can determine the initial probability. Finally, for short thickness, most protons would cross the silicon layer and reach the sensitive region with an energy given by Equation (3). This then needs to be added to the initial

probability to obtain the cumulative probability. Then we must determine the LET of these primary protons appearing in the LET distribution as the direct ionization peak.

### 3.4. Cumulative Probability Calculation

Using our approach, we are then able to determine the cumulative probability of ions reaching the sensitive region. This quantity gives the probability that an ion reaches the sensitive region with an LET greater than a given value. Figure 8 plots these distributions for incident protons with energies ranging from 1 to 10 MeV. For a LET greater than  $2 \text{ MeV}\cdot\text{cm}^2/\text{mg}$ , we observe that the probability to trigger an SEE increases with proton energy. Nevertheless, below  $2 \text{ MeV}\cdot\text{cm}^2/\text{mg}$ , the lowest energies become the main contributors to the cumulative probability. At a very low LET, below  $0.2 \text{ MeV}\cdot\text{cm}^2/\text{mg}$ , the direct ionization peak is the main contributor, and the probability is 3–4 orders of magnitude higher.

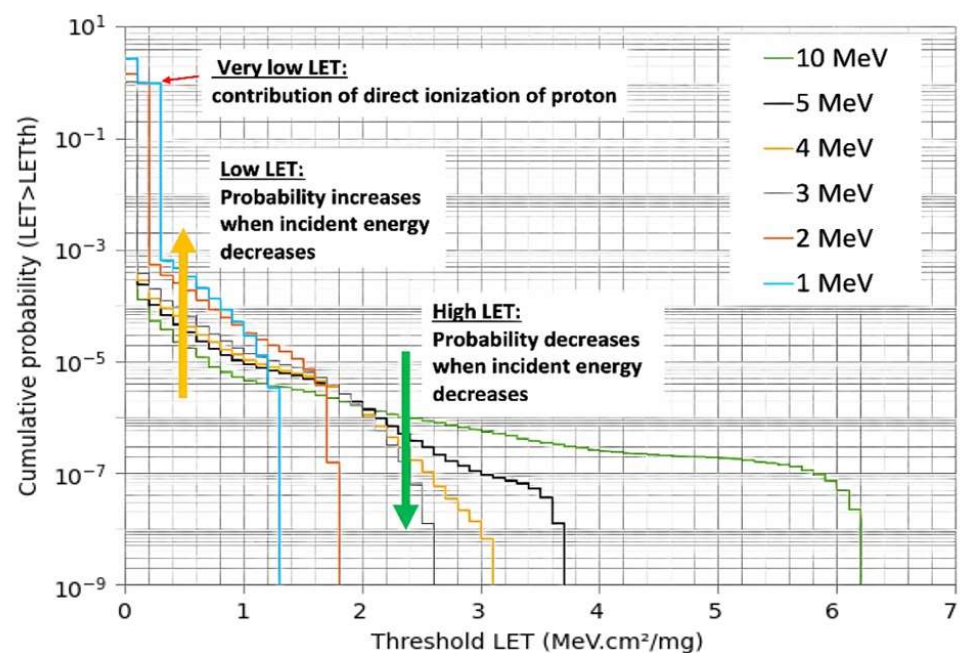


**Figure 8.** Cumulative probability to obtain a silicon recoil with a  $LET > LET_{th}$  for different proton energies. In this example, the BEOL thickness is  $10 \mu\text{m}$ . The sensitive region layer is  $1 \mu\text{m}$ .

This is a very important result since it is generally assumed that when the sensitivity increases (i.e., the threshold LET decreases), the probability to have a recoil decreases, and one must only consider the direct ionization peak. Here, we can clearly see that the decrease in incident energy is associated with an increase in the probability of low-LET recoiling particles. Using this result, we can finally apply Equation (1) and calculate the SEE cross-section.

## 4. Results and Discussion

To validate our method, we took the single-event upset (SEU) experimental results for the 90 nm, 65 nm, and 40 nm SRAMs [28,29] as a reference. We fit the  $\sigma_{HI}(LET)$  with a power law, which can be an alternative of the Weibull shape [30]. Figures 9–11 plot this power law in comparison with experimental  $\sigma_{HI}(LET)$  results. We developed a tool to calculate the SEE cross-section with the methodology presented in the previous section and using Equation (1). These results are plotted in Figures 12–14 together with the experimental SEU cross-section.

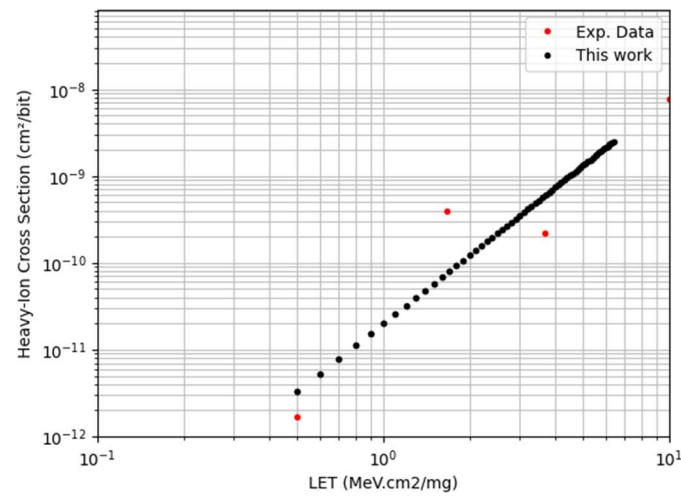


**Figure 9.** Heavy-ion cross-section for 90 nm SRAM fitted with a power law. Experimental data taken from [29].

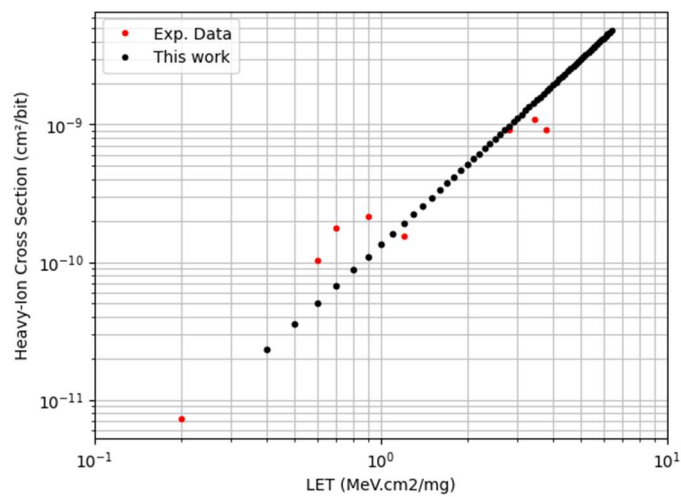


**Figure 10.** Heavy-ion cross-section for 65 nm SRAM fitted with a power law. Experimental data taken from [28].

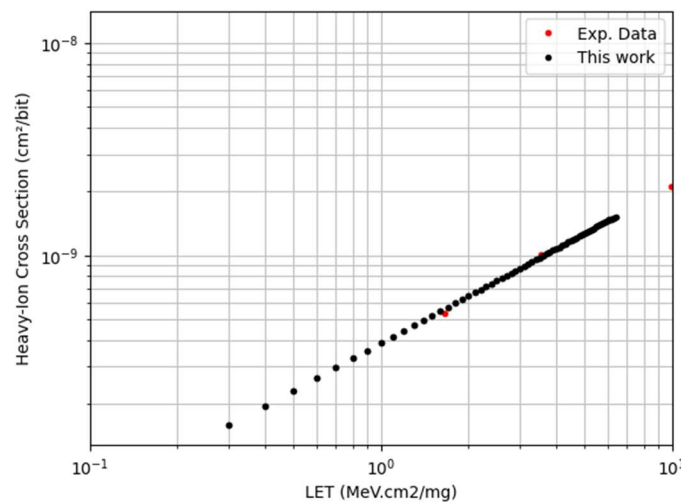


**Figure 11.** Heavy-ion cross-section for 40 nm SRAM fitted with a power law. Experimental data taken from [29].

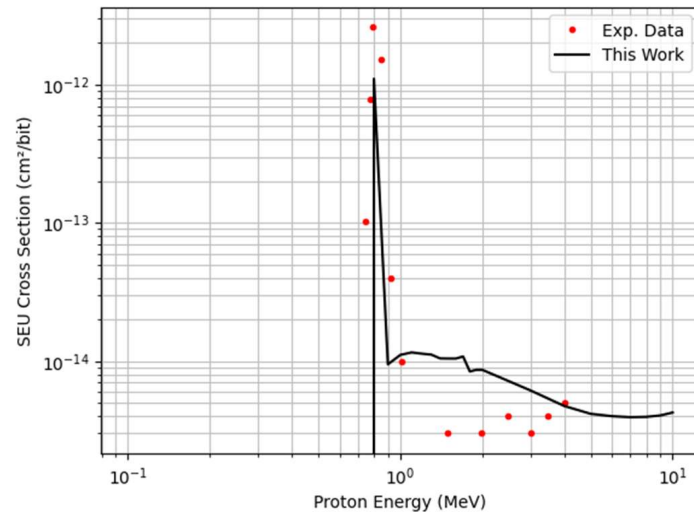


**Figure 12.** SEU cross-section calculation for 90 nm SRAM. Experimental data taken from [29].

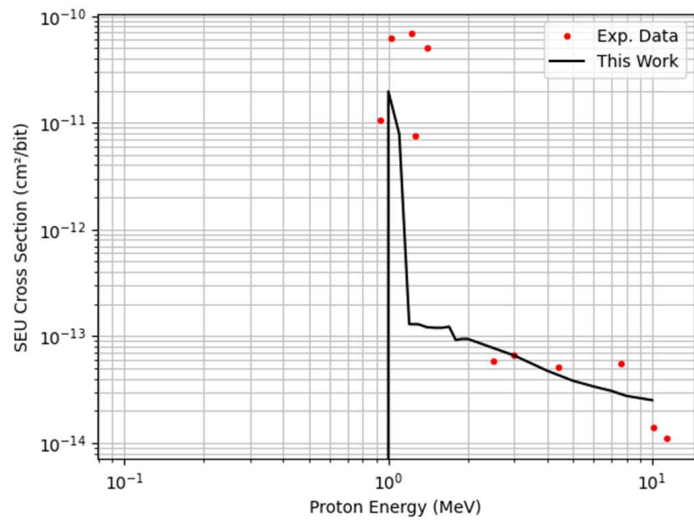


**Figure 13.** SEU cross-section calculation for 65 nm SRAM. Experimental data taken from [28].

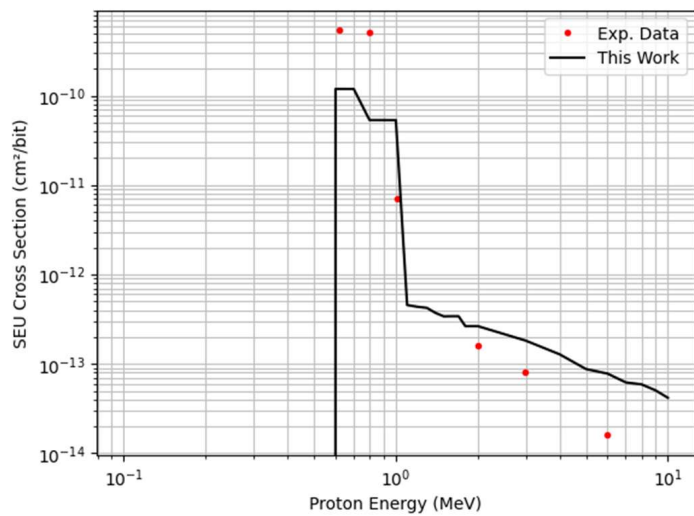


**Figure 14.** SEU cross-section calculation for 40 nm SRAM. Experimental data taken from [29].

For 90 nm, the input parameters are a BEOL thickness of 10  $\mu\text{m}$ , a sensitive region thickness of 2  $\mu\text{m}$ , and a heavy-ion  $\text{LET}_{th}$  of 0.5  $\text{MeV}\cdot\text{cm}^2/\text{mg}$ . At 65 nm, we are us-

ing a BEOL thickness of 15  $\mu\text{m}$ , a sensitive region of 2  $\mu\text{m}$ , and a heavy-ion  $\text{LET}_{th}$  of 0.3  $\text{MeV}\cdot\text{cm}^2/\text{mg}$ . For 40 nm, the BEOL is 6  $\mu\text{m}$ , the sensitive region thickness is 1  $\mu\text{m}$ , and the heavy-ion  $\text{LET}_{th}$  is 0.5  $\text{MeV}\cdot\text{cm}^2/\text{mg}$ . The BEOL thickness was approximated considering the energy loss of the proton in the *Si*, thus making it possible to estimate the energy value of occurrence of the direct ionization peak.

The obtained results consistently align with the experimental data, though not achieving perfect agreement. Nevertheless, our evaluation of the SEU cross-section stands as robust. Our simulation requires only four input parameters, and despite the necessary simplifications in our calculations, including approximations in dimensions for each technology node and composition of the device structure, our results demonstrate a remarkable degree of consistency when compared to the experimental data. Notable, we observe a direct ionization peak around 1 MeV as well as a significant cross-section between 1 and 10 MeV.

Again, below 10 MeV, we have a major contribution of elastic scattering. The results could be improved if we would have had more data about the technology, in particular:

- More information about the BEOL thickness;
- More details about the BEOL composition;
- More experimental data points for heavy ions, especially between 0.2 and 0.8  $\text{MeV}\cdot\text{cm}^2/\text{mg}$ .

When dealing with the calculation of the SEE cross-section, there are a few crucial points to consider:

- To calculate the differential cross-section, we used the DHORIN code, but other tools may be available; however, it is mandatory to consider the Coulomb scattering.
- It is very important to account for the loss of energy of the primary proton, as it will determine the secondary ion energy distribution.
- We must account for the distance that the secondaries will travel before reaching the sensitive region.
- The calculation of the SEE cross-section for protons should not be calculated with a simple-step function, as it may lead to a major discrepancy.

## 5. Conclusions

In modern technologies, the susceptibility for SEE can be very high at a low incident proton energy (below 10 MeV). The main contribution at around 1 MeV is attributed to the direct ionization peak. However, between 1 and 10 MeV, there is also a significant cross-section which should be considered. This cross-section is associated with elastic collisions between incident protons and the nuclei of the matter. The main contribution to this is the Coulomb interaction, which does not occur for neutrons.

We have used a specific optical model to calculate the differential cross-section of the interaction of protons with a silicon nucleus. Results showed that, because the cross-section exhibits a divergence, this will have a significant impact on the LET distribution of ions that reach the sensitive region. Additionally, through a simplified modeling approach using only four input parameters (BEOL layer thickness, sensitive region thickness, technology  $\text{LET}_{th}$ , and HI cross-section data), we were able to compute the SEE cross-section for incident protons. The calculated results demonstrate a good agreement with the experimental data in terms of shape and order of magnitude for different technological nodes. The divergences in concern to the experimental data are related to the simplifications in our calculations, including approximations in the dimensions of each technological node and the composition of the device structure. This agreement provides insights into the underlying mechanisms involved in SEE triggering.

For accurate calculations of the SEE cross-section for protons, we showed that it is important to consider the Coulomb scattering, which can result in significant recoil events. This is especially critical at low energies when the BEOL thickness cannot be negligible in comparison to the range of primary protons. The energy loss of primary protons is a key factor, as it determines the distribution of secondary ion energies. In addition, it is crucial to avoid using a simple-step function to calculate the SEE cross-section; in this work, we

suggest a power or a Weibull law based on experimental data from heavy-ion analysis. It should be noted that the results may vary depending on the amount of heavy-ion data available.

**Author Contributions:** Conceptualization, C.M. and F.W.; methodology, C.M. and F.W.; validation, C.M., F.W., Y.A. and A.M.; formal analysis, C.M. and F.W.; investigation, C.M., F.W. and Y.A.; resources, Y.A., R.G.A. and F.S.; writing—original draft preparation, C.M.; writing—review and editing, F.W., Y.A., A.M., R.G.A., F.S. and J.B.; visualization, C.M., F.W., Y.A., A.M., R.G.A., F.S. and J.B.; project administration, R.G.A. and F.S.; funding acquisition, R.G.A. and F.S. All authors have read and agreed to the published version of the manuscript.

**Funding:** This project has received funding from the European Union’s Horizon 2020 research and innovation program under grant agreement No 101008126.

**Institutional Review Board Statement:** Not applicable.

**Informed Consent Statement:** Informed consent was obtained from all subjects involved in the study.

**Data Availability Statement:** Data are contained within the article.

**Conflicts of Interest:** The authors declare no conflict of interest.

## References

- Lawrence, R.K.; Ross, J.F.; Haddad, N.F.; Reed, R.A.; Albrecht, D.R. Soft Error Sensitivities in 90 nm Bulk CMOS SRAMs. In Proceedings of the 2009 IEEE Radiation Effects Data Workshop, Quebec, QC, Canada, 20–24 July 2009; pp. 123–126. [\[CrossRef\]](#)
- Liao, W.; Ito, K.; Abe, S.-I.; Mitsuyama, Y.; Hashimoto, M. Characterizing Energetic Dependence of Low-Energy Neutron-Induced SEU and MCU and Its Influence on Estimation of Terrestrial SER in 65-nm Bulk SRAM. *IEEE Trans. Nucl. Sci.* **2021**, *68*, 1228–1234. [\[CrossRef\]](#)
- Cannon, J.M.; Loveless, T.D.; Estrada, R.; Boggs, R.; Lawrence, S.P.; Santos, G.; McCurdy, M.W.; Sternberg, A.L.; Reising, D.R.; Finzell, T.; et al. Electrical Measurement of Cell-to-Cell Variation of Critical Charge in SRAM and Sensitivity to Single-Event Upsets by Low-Energy Protons. *IEEE Trans. Nucl. Sci.* **2021**, *68*, 815–822. [\[CrossRef\]](#)
- Wrobel, F.; Aguiar, Y.; Marques, C.; Lerner, G.; García Alía, R.; Saigné, F.; Boch, J. An Analytical Approach to Calculate Soft Error Rate Induced by Atmospheric Neutrons. *Electronics* **2023**, *12*, 104. [\[CrossRef\]](#)
- Lüdeke, S.; Cardenás, G.D.; Hajdas, W.; Jaatinen, J.; Kettunen, H.; Poivey, C.; Rossi, M.; Tanios, B.; Vogiatzi, S.M.; Javanainen, A. Proton Direct Ionization in Sub-Micron Technologies: Test Methodologies and Modeling. *IEEE Trans. Nucl. Sci.* **2023**, *70*, 667–677. [\[CrossRef\]](#)
- Hubert, G.; Bougerol, A.; Miller, F.; Buard, N.; Anghel, L.; Carriere, T.; Wrobel, F.; Gaillard, R. Prediction of transient induced by neutron/proton in CMOS combinational logic cells. In Proceedings of the 12th IEEE International On-Line Testing Symposium (IOLTS’06), Lake Como, Italy, 10–12 July 2006; p. 9. [\[CrossRef\]](#)
- Sun, W.; Watanabe, Y.; Sukhovitskiĭ, E.S.; Iwamoto, O.; Chiba, S. Evaluation of Cross Sections for Neutrons and Protons up to 200 MeV on Silicon Isotopes. *J. Nucl. Sci. Technol.* **2002**, *39*, 120–123. [\[CrossRef\]](#)
- Akkerman, A.; Barak, J.; Yitzhak, N.M. Role of Elastic Scattering of Protons, Muons, and Electrons in Inducing Single-Event Upsets. *IEEE Trans. Nucl. Sci.* **2017**, *64*, 2648–2660. [\[CrossRef\]](#)
- Rodbell, K.P.; Protons, L.-E. Low-Energy Protons—Where and Why “Rare Events” Matter. *IEEE Trans. Nucl. Sci.* **2020**, *67*, 1204–1215. [\[CrossRef\]](#)
- Sierawski, B.D.; Pellish, J.A.; Reed, R.A.; Schrimpf, R.D.; Warren, K.M.; Weller, R.A.; Mendenhall, M.H.; Black, J.D.; Tipton, A.D.; Xapsos, M.A.; et al. Impact of Low-Energy Proton Induced Upsets on Test Methods and Rate Predictions. *IEEE Trans. Nucl. Sci.* **2009**, *56*, 3085–3092. [\[CrossRef\]](#)
- Caron, P.; Inguibert, C.; Artola, L.; Ecoffet, R.; Bezerra, F. Physical Mechanisms of Proton-Induced Single-Event Upset in Integrated Memory Devices. *IEEE Trans. Nucl. Sci.* **2019**, *66*, 1404–1409. [\[CrossRef\]](#)
- Alía, R.G.; Tali, M.; Brugger, M.; Cecchetto, M.; Cerutti, F.; Cononetti, A.; Danzeca, S.; Esposito, L.; Fernandez-Martinez, P.; Gilardoni, S.; et al. Direct Ionization Impact on Accelerator Mixed-Field Soft-Error Rate. *IEEE Trans. Nucl. Sci.* **2020**, *67*, 345–352. [\[CrossRef\]](#)
- Cononetti, A.; Alía, R.G.; Wang, J.; Tali, M.; Cecchetto, M.; Cazzaniga, C.; Javanainen, A.; Saigne, F.; Leroux, P. Assessment of Proton Direct Ionization for the Radiation Hardness Assurance of Deep Submicron SRAMs Used in Space Applications. *IEEE Trans. Nucl. Sci.* **2021**, *68*, 937–948. [\[CrossRef\]](#)
- Petersen, E.L. Approaches to proton single-event rate calculations. *IEEE Trans. Nucl. Sci.* **1996**, *43*, 496–504. [\[CrossRef\]](#)
- Jun, I.; Xapsos, M.; Messenger, S.; Burke, E.; Walters, R.; Summers, G.; Jordan, T. Proton nonionizing energy loss (NIEL) for device applications. *IEEE Trans. Nucl. Sci.* **2003**, *50*, 1924–1928. [\[CrossRef\]](#)
- Alía, R.G.; Cononetti, A.; Bilko, K.; Cecchetto, M.; Datzmann, G.; Fiore, S.; Girard, S. Heavy Ion Energy Deposition and SEE Intercomparison Within the RADNEXT Irradiation Facility Network. *IEEE Trans. Nucl. Sci.* **2023**, *70*, 1596–1605. [\[CrossRef\]](#)

17. Leroy, C.; Rancoita, P.G. Principles of radiation interaction in matter and detection. In *World Scientific*, 2nd ed.; World Scientific Pub Co Pte Ltd.: Singapore, 2009; pp. 696–701. [[CrossRef](#)]
18. Wrobel, F. Fundamentals on radiation-matter interaction. In Proceedings of the 2005 8th European Conference on Radiation and Its Effects on Components and Systems, Cap d'Agde, France, 19–23 September 2005; pp. 10–11.
19. Vial, C.; Palau, J.M.; Gasiot, J.; Calvet, M.C.; Fourtine, S. A new approach for the prediction of the neutron-induced SEU rate. *IEEE Trans. Nucl. Sci.* **1998**, *45*, 2915–2920. [[CrossRef](#)]
20. Autran, J.-L.; Munteanu, D. *Soft Errors: From Particles to Circuits*; Taylor & Francis/CRC Press: Abingdon, UK, 2015; pp. 117–125.
21. Palau, J.-M.; Hubert, G.; Coulie, K.; Sagnes, B.; Calvet, M.-C.; Fourtine, S. Device simulation study of the SEU sensitivity of SRAMs to internal ion tracks generated by nuclear reactions. *IEEE Trans. Nucl. Sci.* **2001**, *48*, 225–231. [[CrossRef](#)]
22. Tavernier, S. Interactions of particles in matter. In *Interactions of Particles in Matter*; Springer: Berlin/Heidelberg, Germany, 2009; pp. 23–53.
23. International Atomic Energy Agency—Nuclear Data Section. Available online: <https://www-nds.iaea.org> (accessed on 10 December 2023).
24. Calvel, P.; Barillot, C.; Lamothe, P.; Ecoffet, R.; Duzellier, S.; Falguere, D. An empirical model for predicting proton induced upset. *IEEE Trans. Nucl. Sci.* **1996**, *43*, 2827–2832. [[CrossRef](#)]
25. Wrobel, F. Detailed history of recoiling ions induced by nucleons. *Comput. Phys. Commun.* **2007**, *178*, 88–104. [[CrossRef](#)]
26. Raynal, J. CEA Saclay Report No. CEA-N-2772. ICTP International Seminar Course, IAEA, Italy, 1994. Available online: <https://www.scrip.org/reference/ReferencesPapers?ReferenceID=1459220> (accessed on 10 December 2023).
27. Ziegler, J.F. TRIM. The Transport of Ions in Matter. Available online: <http://www.srim.org> (accessed on 10 December 2023).
28. Sierawski, B.D.; Warren, K.M.; Reed, R.A.; Weller, R.A.; Mendenhall, M.M.; Schrimpf, R.D.; Baumann, R.C.; Zhu, V. Contribution of low-energy ( $\ll 10$  MeV) neutrons to upset rate in a 65 nm SRAM. In Proceedings of the 2010 IEEE International Reliability Physics Symposium, Anaheim, CA, USA, 2–6 May 2010; pp. 395–399. [[CrossRef](#)]
29. Coronetti, A.; Cecchetto, M.; Wang, J.; Tali, M.; Martinez, P.F.; Kastriotou, M.; Papadopoulou, A.; Bilko, K.; Castellani, F.; Sacristan, M.; et al. SEU characterization of commercial and custom-designed SRAMs based on 90 nm technology and below. In Proceedings of the 2020 IEEE Radiation Effects Data Workshop (in conjunction with 2020 NSREC), Santa Fe, NM, USA, 29 November–30 December 2020; pp. 1–8. [[CrossRef](#)]
30. Wrobel, F.; Touboul, A.D.; Pouget, V.; Dilillo, L.; Lorfèvre, E.; Saigné, F. The Power Law Shape of Heavy Ions Experimental Cross Section. *IEEE Trans. Nucl. Sci.* **2017**, *64*, 427–433. [[CrossRef](#)]

**Disclaimer/Publisher's Note:** The statements, opinions and data contained in all publications are solely those of the individual author(s) and contributor(s) and not of MDPI and/or the editor(s). MDPI and/or the editor(s) disclaim responsibility for any injury to people or property resulting from any ideas, methods, instructions or products referred to in the content.